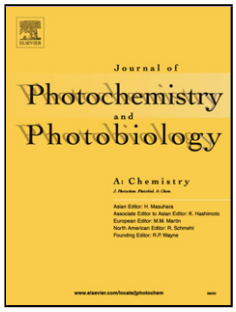

Title: Selective Detection of Human Serum Albumin by Near Infrared Emissive Fluorophores: Insights into Structure-property Relationship

Authors: Rajib Choudhury, Siddhi Rajeshbhai Patel, Anindya Ghosh

PII: S1010-6030(18)31831-8
DOI: https://doi.org/10.1016/j.jphotochem.2019.02.038
Reference: JPC 11737

To appear in: *Journal of Photochemistry and Photobiology A: Chemistry*

Received date: 16 December 2018
Revised date: 14 February 2019
Accepted date: 28 February 2019

Please cite this article as: Choudhury R, Rajeshbhai Patel S, Ghosh A, Selective Detection of Human Serum Albumin by Near Infrared Emissive Fluorophores: Insights into Structure-property Relationship, *Journal of Photochemistry and amp; Photobiology, A: Chemistry* (2019), https://doi.org/10.1016/j.jphotochem.2019.02.038

Selective Detection of Human Serum Albumin by Near Infrared Emissive Fluorophores: Insights into Structure-property Relationship

Rajib Choudhury*[§], Siddhi Rajeshbhai Patel[§], Anindya Ghosh[†]

[§] Department of Physical Sciences, Arkansas Tech University, Russellville, Arkansas, 72801, United States.

[†] Department of Chemistry, University of Arkansas, Little Rock, Arkansas, 72204

[*]Email: rchoudhury@atu.edu; Telephone 479-356-2028; Fax 479-964-0837

Graphical abstract

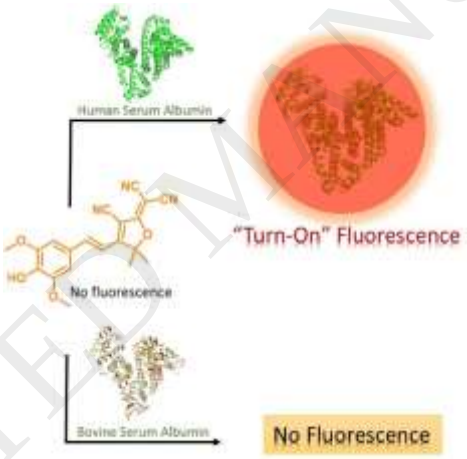

Highlights

pH dependent modulation of intramolecular charge transfer has been reported

Selective detection of human serum albumin in 'turn-on' fashion was demonstrated

The effect of intermolecular interactions in protein sensing was demonstrated

A lower detection limit was obtained by manipulating the charge transfer property of the fluorophores

Abstract

Two donor-acceptor fluorophores were prepared and tested for quantitative determination of HSA in aqueous samples. Fluorophores were non-emissive in polar solvents due to energy loss via non-radiative decays. Complexation of the fluorophores with HSA resulted multi-fold enhancement of emission in the red-near infrared (NIR) region. The emission intensity was linearly correlated to the amount of protein in the solution, which enabled us to develop calibration graphs for quantitative estimation of HSA in synthetic urine samples. Between the two fluorophores, the methoxy substituted fluorophore 1 selectively recognized HSA. It exhibited remarkable fluorescence enhancement with HSA over bovine serum albumin (BSA) and other globular proteins. The selective sensing aptitude of 1 was attributed to its restricted motions in the protein's microenvironment due to multiple non-covalent interactions, preventing energy loss by radiationless decay. The different recognition properties of the fluorophores were estimated by the steady-state fluorescence and molecular docking studies. These findings indicate that this class of fluorophores can be useful for quantitative estimation of HSA in biological urine and blood samples in clinical practice.

Keywords

Human Serum Albumin, Intramolecular charge transfer, Turn-on fluorescence

Introduction

Human serum albumin (HSA) is the major constituent of blood plasma.[1-5] About 50% of the total serum protein content is albumin. It serves as a biomarker for a wide range of health conditions

such as renal disease, coronary artery disease, stroke, liver, and kidney failure.[1-5] Normally, the amount of HSA in serum is ~35-50 g/L and less than 20 mg/L in the urine samples of healthy persons.[6] However, these amounts might vary due to adverse health conditions. For example, HSA level in urine between 30-300 mg/L indicates risk of cardiovascular or kidney disease, a term is known as microalbuminuria.[2, 7-8] Amount of HSA more than 300 mg/L in urine is diagnosed as macroalbuminuria, a condition when a kidney disease has progressed to an irreversible kidney failure.[9] Moreover, a very low concentration of HSA in blood serum might indicate liver cirrhosis, liver failure, and chronic hepatitis.[1] Therefore, selective and quantitative determination of HSA in body fluids is of immense clinical importance.

In the past, several tools such as spectrophotometry, immunoelectrophoresis, immunoturbidimetry, enzyme-linked immunosorbent assay (ELISA), radioimmunoassay, and LC-MS/MS have been developed for the quantitative determination of HSA in biological fluids.[10-17] Recently, external fluorescent probe based detection technique has attracted much attention of the bioanalytical chemists.[18-22] Fluorescent based tools are cost-effective, non-invasive, and rapid in nature. However, a suitable fluorophore is always required for the detection and quantification of HSA in complex biological samples. In this context, small molecule fluorophores that spontaneously bind with HSA and strongly emit as a result of the strong supramolecular association are very promising. Especially, fluorophores that emit in the near infrared (NIR) region are good candidates as they remain minimally disturbed by the fluorescence of the other biomolecules.[23-25]

Several far-red and NIR emitting fluorophores have been reported in literature. Although each fluorophore has some distinct merits over another, some of the common demerits of NIR fluorophores are, poor aqueous solubility, aggregation-caused quenching, marginal output signal, and insufficient detection limit.[26-28] Above all the most frequently encountered demerit is lack of selectivity of the fluorophores for HSA.[11, 20] Therefore, a fluorophore capable of detecting a target biomarker in selective fashion is highly desirable. Selective detection and quantification would be useful for the accurate determination of HSA in biological samples in clinical diagnosis operations. Herein, we have prepared and examined two donor-acceptor fluorophores for selective detection and quantification of HSA in buffer as well as in synthetic urine solutions. A strong electron acceptor, tricyanofuran (TCF), was conjugated with an ionizable phenol derivative (the electron donor moiety) by an alkenyl-double bond to obtain a push-pull based π-electron system.[24, 29]

Fluorophores were soluble in water and emitted in the far-red to NIR region of the spectrum. Due to efficient intramolecular charge transfer (ICT) and the subsequent formation of the low lying energy states the fluorescence was heavily quenched in polar solvents.[30-31] Fluorescence was recovered upon complexation of the fluorophores with HSA, which resulted 1-3 mg/L Limit of Detection (LOD) in synthetic urine solutions. Interestingly, one fluorophore selectively responded to HSA with rapid enhancement of the fluorescence intensity. By employing steady-state fluorescence, site-specific binding assays, and molecular docking studies the underlying mechanism of the high selectivity was examined, and it was attributed to the size/shape of the fluorophore and the specific van der Waals interactions between the fluorophore and the amino acid residues in the binding site. High complexation affinity and selectivity of the fluorophore toward HSA suggest that it can be used for selective detection and quantification of HSA in biological samples such as urine and blood.

Experimental

Materials and methods

Bio-macromolecules (human serum albumin, bovine serum albumin, β-lactoglobulin, γ-globulin, pepsin, trypsin, lysozyme, insulin, hemoglobin, and chicken egg albumin), and synthetic urine were purchased from Sigma-Aldrich. Malononitrile, 3-hydroxy-3-methylbutan-2-one, 4-hydroxy-3,5-dimethoxybenzaldehyde, 4-hydroxybenzaldehyde, sodium ethoxide, ammonium acetate, ibuprofen, buffer solutions: pH 4.0, 6.0, 7.0, 7.4, 9.0, 10.0, 11.0 and phenylbutazone were purchased from Sigma-Aldrich and used without further purifications. Hexane, ethyl acetate, acetone, acetonitrile, dichloromethane, dimethylformamide, dimethyl sulfoxide, methyl alcohol, and ethyl alcohol were of spectrophotometric grade. Silica gel (40-63 μm), thin layer chromatography plates (TLC silica gel 60 F254), and glycerol were obtained from VWR. Deuterated dimethyl sulfoxide (DMSO-d_6) was purchased from Cambridge Isotope Laboratories, Inc (Cambridge, MA).Water was purified using a deionization system.

NMR spectra were recorded on a JEOL NMR spectrometer operating at 400 MHz for ^{1}H NMR and 100.6 MHz for ^{13}C NMR, respectively. Acquired data were processed on a windows computer with Delta 5.2.1 program. Chemical shifts are represented in parts per million (ppm) and referenced to DMSO solvent peak. All the absorption spectra were recorded on a Shimadzu UV-2501 PC spectrophotometer. All the emission spectra were collected using a LS 55 Luminescence

Spectrometer (PerkinElmer). To record absorption and emission spectra, a stock solution of the fluorophore in DMSO was added in respective buffer solutions. The amount of DMSO in buffer solutions was always 1% or less. Infrared spectra were recorded on a Bruker Alpha FT-IR Spectrometer. For each sample, 16 spectra were collected at a 4 cm^{-1} spectral resolution with a spectral width of 4000 to 700 cm^{-1}. Background subtraction and signal frequency determination were performed on the Opus/Mentor software.

Molecular docking was carried out on a Windows-OS computer (64-bit) with 3.30 GHz processor and 8.00 GB of RAM on Vina 1.1.2 program.[32] 3D coordinates of the fluorophores (scheme 1) were constructed on Chem 3D program and optimized with molecular mechanics (MM2) force field. Crystal structure of the HSA was obtained from protein data bank (PDB code: 2BXC). AutoDock Tools 1.5.6 was used for assigning the docking area and preparing the input files in pdbqt format, which is a modified PDB format with information about atomic charges, atom type definitions, and topological information for the fluorophores. During input file preparation, Gasteiger partial charges were added to the fluorophores; non-polar hydrogens were merged, and torsional rotatable and non-rotatable bonds were defined. All the acyclic single bonds were made rotatable; double and triple bonds were assigned as non-rotatable. All other docking parameters were kept at their default values. Dimension of the search space was set to 34 × 34 × 32 $Å^3$ with 1.0 Å grid spacing. The exhaustiveness of each docking was set at 20 and the seed was varied randomly as generated by the program.

Molecular docking predicts conformations of small ligands or drugs when they are docked within a protein. Usually docking calculations use scoring functions such as, geometric and energetic functions, as well as empirical functions which are unique to each program. To gain more precise results in the binding site determination and the rankings of the conformations of the fluorophores reported in this article, first a docking run was carried out with a known drug@HSA complex with the same parameters that have been used throughout this study. Phenylbutazone was selected as a drug candidate and docked with HSA, and the best pose obtained from the docking was compared with the reported crystal structure of the phenylbutazone@HSA complex. An identical binding site (Sudlow I) was obtained from the docking run, suggesting that a comprehensive understanding of the HSA-fluorophore structures can be obtained from the docking calculations reported in this article.

Results and discussion

Fluorophores were synthesized by following literature reports (scheme 1).[22, 33] First, 3-hydroxy-3-methylbutan-2-one was refluxed with malononitrile in presence of sodium ethoxide under nitrogen atmosphere to obtain 2-(3-cyano-4,5,5-trimethylfuran-2(5H)-ylidene)malononitrile (compound **A**, TCF acceptor unit). Acceptor **A** was then treated with 4-hydroxy-3,5-dimethoxybenzaldehyde (**B**) in presence of a weak base at 50 ^{o}C to obtain (*E*)-2-(3-cyano-4-(4-hydroxy-3,5-dimethoxystyryl)-5,5-dimethylfuran-2(5H)-ylidene)malononitrile (fluorophore **1)**. Similarly, fluorophore **2** was obtained upon treatment of 4-hydroxybenzaldehyde (**C**) with acceptor **A** under the N_2 atmosphere. Intermediate **A** was purified by recrystallization from ethanol, and the final compounds were purified by silica gel chromatography using hexane and ethyl acetate as eluents to yield crystalline solids. Both fluorophores were soluble in water, a property which is highly desirable for applications in biological studies.

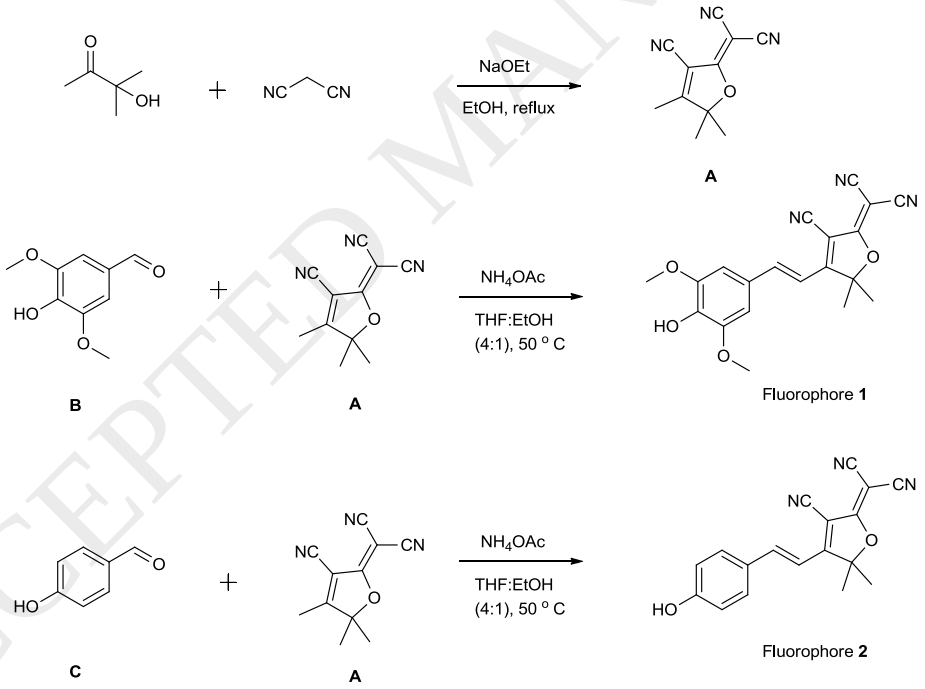

Scheme 1. Synthesis of the fluorophores.

The yield of the final condensation reaction was 35% and 40% for **1** and **2**, respectively. The final products were characterized by IR and NMR (^{1}H and ^{13}C) spectroscopy and elemental analysis (figure S1-S4). IR spectra of **1** and **2** displayed signals at ~2220 cm^{-1}, indicating presence of nitrile

stretching frequencies. Broad signals corresponding to –OH groups were also observed at ~3309 cm^{-1} and ~3356 cm^{-1} for **1** and **2**, respectively. In the ^{1}H NMR spectrum of **1**, signal at 3.82 ppm confirmed presence of –OMe groups attached to a phenyl moiety. In DMSO broad downfield shifted signals in the range of 9.5-11.0 ppm confirmed presence of phenolic –OH groups in **1** and **2** (figure S1 and S3). For both the fluorophores, selectivity to all-trans isomer of Knoevenagel condensation was very high within the limits of the NMR detection. Presence of vinylic hydrogens was confirmed by calculating coupling constant, and it was found to be 16 Hz for both **1** and **2**.

Fluorophore **1** displayed moderate positive solvatochromism; the absorption maxima (λ_{max}) shifted to longer wavelengths with increase in polarity of the solvents (figure 1a and figure S5). In ethyl acetate ($\varepsilon = 6.02$) λ_{max} of absorption was at 470 nm, which shifted to 475 nm in moderately polar solvent DCM ($\varepsilon = 8.93$). Further bathochromic shifts were observed in more polar solvents such as DMSO, acetone, ACN, methanol, and ethanol. As shown in figure 1a, multiple broad absorption signals were observed in polar solvents, both in the high energy and low energy regions of the electromagnetic spectrum. In deionized water and phosphate buffer (pH = 7.4) relatively narrow absorption bands were observed centered around 630 nm.

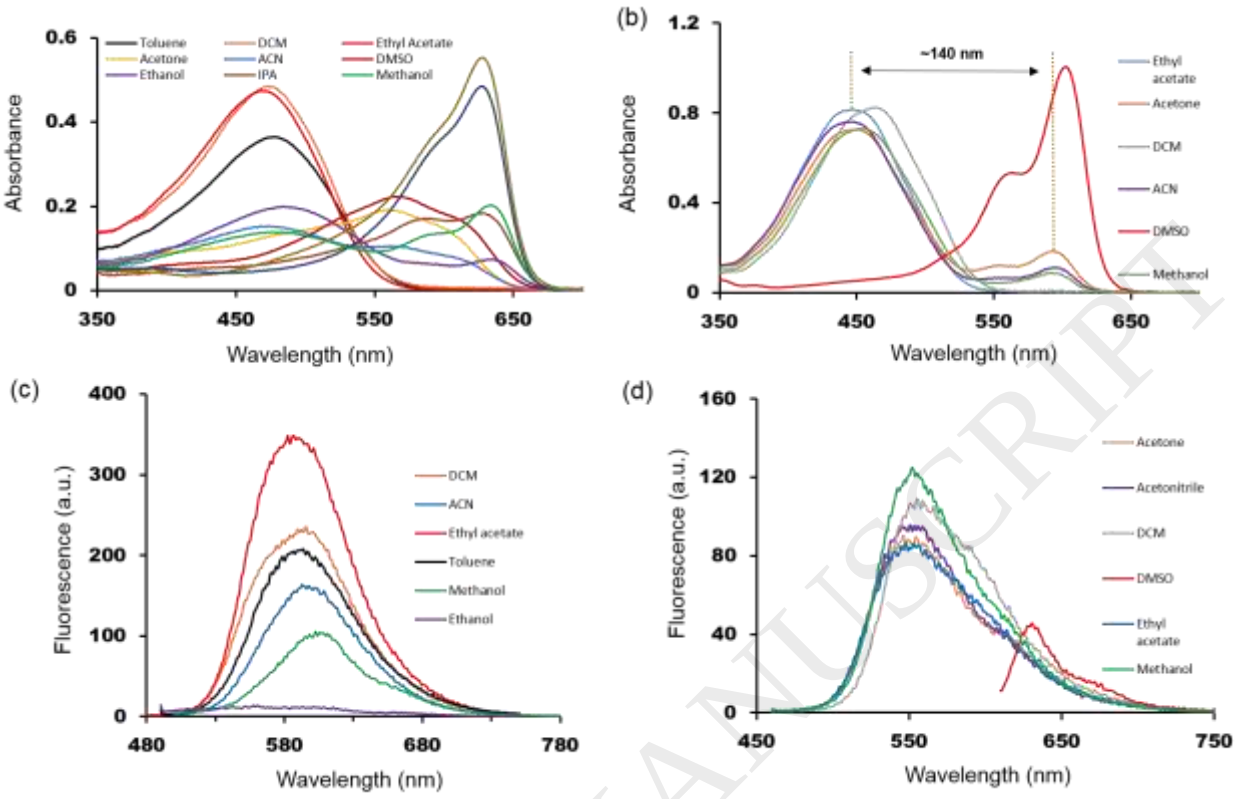

Figure 1. (a) Absorption spectra of fluorophore **1** in various solvents. [**1**] = 1.0×10^{-5} M. Aqueous solution contains 1% DMSO. (b) Absorption spectra of fluorophore **2** in various solvents. [**2**] = 1.0×10^{-5} M. Aqueous solution contains 1% DMSO (c) Fluorescence spectra of **1** in various solvents. [**1**] = 1.0×10^{-5} M. Aqueous solution contains 1% DMSO. (d) Fluorescence spectra of **2** in various solvents. [**2**] = 1.0×10^{-5} M. Aqueous solution contains 1% DMSO.

Fluorophore **2** also showed positive solvatochromism (figure 1b and figure S5). In ethyl acetate λ_{max} was at 450 nm; it shifted to 470 nm in DCM. But, in methanol, acetonitrile, and acetone, longer wavelength absorptions were observed with a bathochromic shift of ~ 140 nm. The intensities ($\varepsilon \approx 20000$ $Lmol^{-1}cm^{-1}$) of the absorption bands corresponding to the polar solvent stabilized energy states were lower than that of the bands observed in nonpolar solvents ($\varepsilon \approx 82000$ $Lmol^{-1}cm^{-1}$ in DCM) such as ethyl acetate and DCM (figure 1b). However, in DMSO a very intense absorption band ($\varepsilon \approx 200000$ $Lmol^{-1}cm^{-1}$) was observed at 605 nm along with a 'shoulder' at ~565 nm.

The fluorescence properties of **1** and **2** were also investigated in various nonpolar and polar solvents. Significant solvent effect was observed for **1** at high energy emission maxima; 20 nm

bathochromic shift and reduced intensities were recorded when solvent was switched from ethyl acetate to DCM to methanol (figure 1c). However, no such sequential red shift was observed at low energy emissions centered ~ 650 nm in solvents such as acetone, DMSO, and acetonitrile (figure S5). All the emissions were heavily quenched, most likely due to energy loss from the solvent stabilized charge transfer states *via* non-radiative pathways.[31] Emission maxima of **2** was not very sensitive to the polarity of the solvents; it did not display any noticeable trend in red shifts. As shown in figure 1d, all the emission bands were centered ~555 nm. However, when highly polar DMSO was used as a solvent, a low intense narrow emission signal along with a 'shoulder' peak was observed at 635 nm.

Phenolic compounds possess interesting optical properties.[34] Neutral phenol and phenolate anion emit at different wavelengths.[34] The pK_a of phenol is 9.98, but if two electron withdrawing methoxy groups are attached at the ortho positions, the pK_a can be lowered by stabilizing the negative charge on the phenolate anion. As shown in figure 2a, the absorption maxima at 463 nm was attributed to the neutral form of **1**. It gradually decreased upon increasing the pH from 4.0 – 6.0 – 7.4. It completely disappeared at pH 7.4, indicating presence of only deprotonated form. However, at pH 6.0, along with the high energy band at 463 nm, a broad split peak was observed centered ~ 615 nm. With increase in pH the band bathochromically and hyperchromically shifted to 630 nm as a narrow band (figure 2a). The intensity of the absorption maxima was slightly higher at pH 9.0 and 10.0 than at pH 7.4, suggesting growing deprotonated forms at higher pH values. Moreover, similar shapes and intensities of the absorption bands at pH 7.4, 9.0, and 10.0 suggest that **1** exists predominately in the deprotonated form at physiological buffer (pH = 7.4). Emission property of **1** was also studied in water at different pH values (figure 2c). The emission of the neutral form was broader and more intense than the deprotonated form. The Stokes' shift of the neutral form was 144 nm, whereas the deprotonated form displayed 26 nm of Stokes' shift.

Similar optical properties were observed for **2**. At pH 4.0 and 6.0, the absorption maxima at 448 nm was attributed to the neutral form, though a small amount of deprotonated form exists at pH 6.0 as indicated by a band at 575 nm (figure 2b). At pH 7.4, both neutral and deprotonated form exit; the amount of deprotonated form (ε = 36900 $Lmol^{-1}cm^{-1}$) was higher than that of the neutral form (ε = 20800 $Lmol^{-1}cm^{-1}$). Upon increasing the pH of the solution to 9.0, only the band corresponding to the deprotonated form (ε = 74200 $Lmol^{-1}cm^{-1}$ at 575 nm) was observed, whose

intensity further increased at pH 10.0 (ε = 91400 $Lmol^{-1}cm^{-1}$ at 575 nm). These observations suggest that the 575 nm absorption band arises from the deprotonated form of the fluorophore and it is significantly red shifted (~127 nm) due to different electron donating abilities of phenolate and phenol donors.

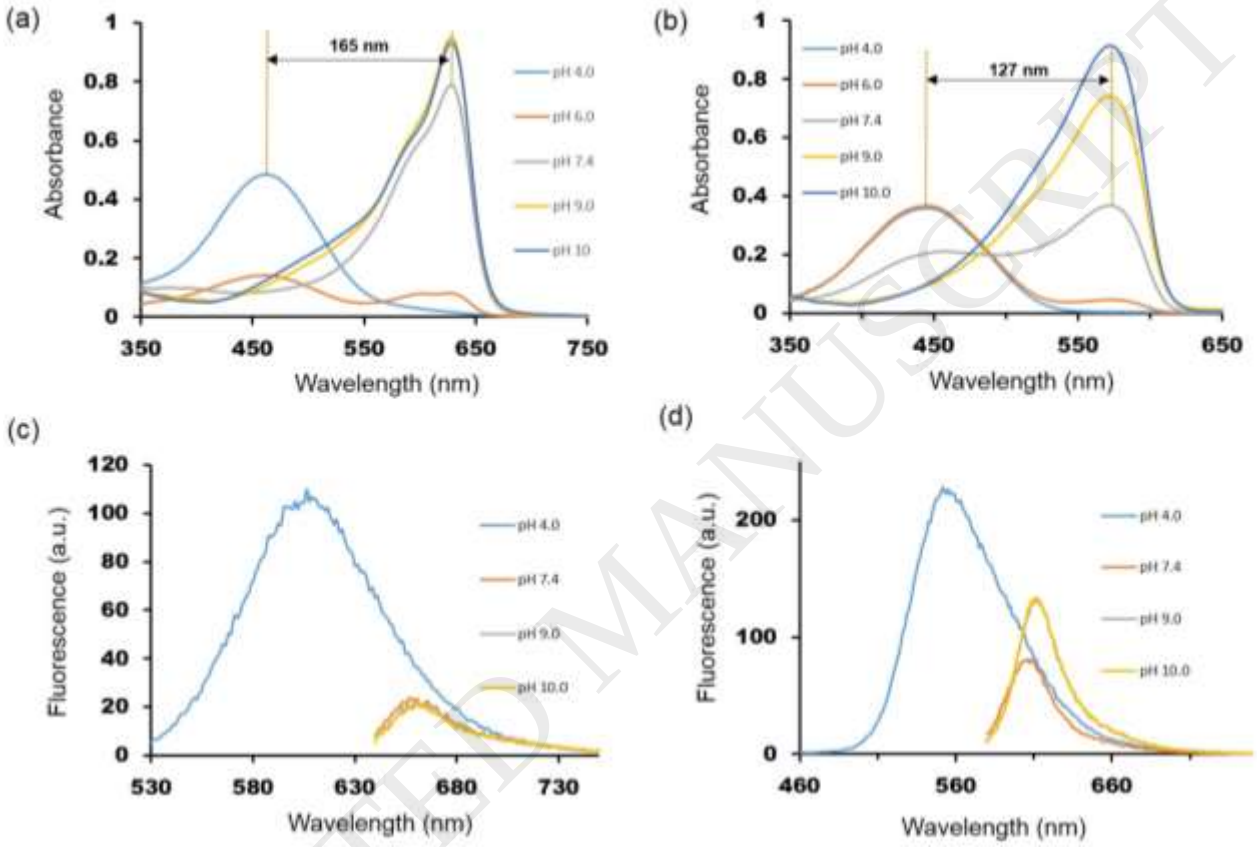

Figure 2. (a) Absorption spectra of **1** in water at different pH. (b) Absorption spectra of **2** in water at different pH. (c) Fluorescence spectra of **1** in water at different pH. (d) Fluorescence spectra of **2** in water at different pH. All the aqueous solutions contain 1% DMSO. [**1**] = 1.0×10^{-5} M; [**2**] = 1.0×10^{-5} M.

Like **1**, the neutral form of **2** was more emissive than the deprotonated form, and it displayed 114 nm Stokes' shift (figure 2d). Emission intensities were higher and more bathochromically shifted at pH 9.0 and 10.0 (Stokes' shift 40 nm) than at pH 7.4 (Stokes' shift 35 nm). The dramatic change in the absorption and emission spectra of **1** and **2** upon increasing the pH of the solution was accounted for the formation of the phenolate ion. Moreover, a phenolate ion with excess electron density on oxygen can better donate electrons in the conjugated D-π-A system than a neutral -OH

group. Hence, a low energy emission band arises for the anionic form in water at higher pH values.[34]

As shown in the previous sections, upon increasing the solvent polarity, the emissions of **1** and **2** were quenched. The mechanism of the quenching may involve loss of the excited state energy (ICT states) via non-radiative pathways.[31, 35] To confirm whether the microenvironment had any role in the fluorescence loss of the compounds, the emission spectra of the fluorophores were recorded in methanol and methanol-glycerol mixture (figure 3). Glycerol is a viscous liquid (viscosity 950 cP at 25 ^{o}C); upon increasing the glycerol ratio in methanol-glycerol mixture, a systematic fluorescence enhancement was observed for both **1** and **2**. A 3-fold fluorescence enhancement for **1** and 1.5-fold for **2** was observed in 1:1 methanol-glycerol mixture (figure 3), indicating reduced rotational motions in viscous microenvironment.[31, 36]

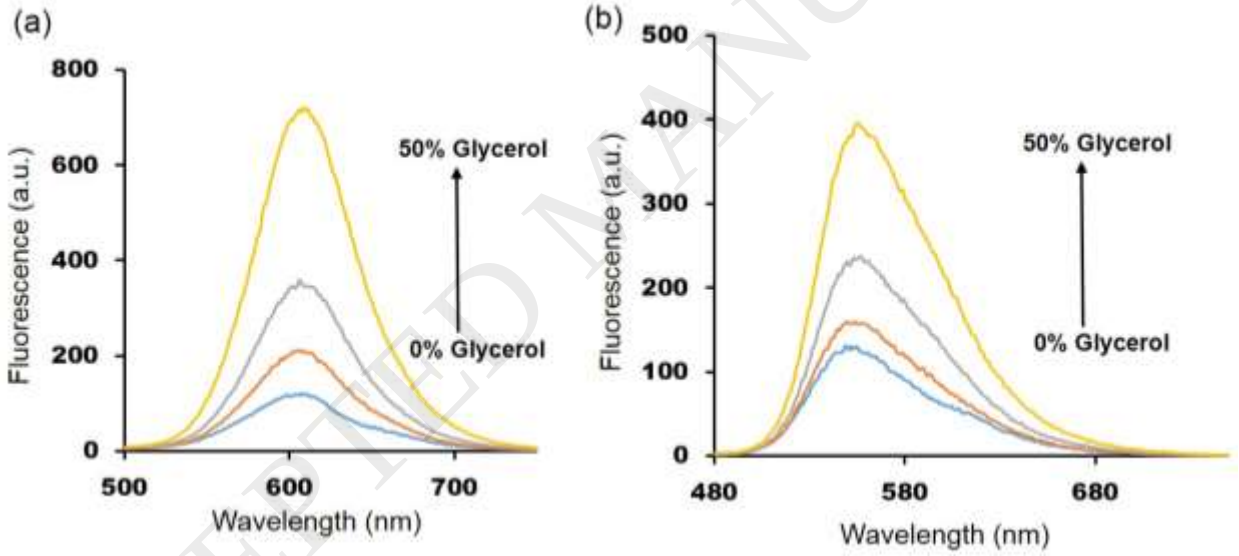

Figure 3. (a) Fluorescence spectra of **1** (10 µM) in different ratios of methanol-glycerol mixtures. (b) Fluorescence spectra of **2** (10 µM) in different ratios of methanol-glycerol mixtures.

The fluorescence enhancement within the viscous microenvironment prompted us to investigate the complexation of **1** and **2** with HSA and BSA in buffer (1 mM, pH = 7.4). As shown in figure 4, 10 nm and 35 nm red shift was observed for **1** and **2**, respectively, when one equivalent of HSA was added into a buffer solution of the fluorophore, implying binding of the fluorophore within the protein's binding pocket (figure S6). In this context, the 35 nm red shift for **2** was exemplary. The color change was even discernible to naked eyes (figure 4b; inset). Since this color change

occurred in a buffer solution of constant pH, it is likely that a proton exchange took place between **2** and the HSA. Moreover, the intensity of the absorption maxima corresponding to the neutral form (at 448 nm) significantly decreased in the presence of one equivalent of HSA (figure 4b), suggesting disappreance of the neutral form and formation a new equilibrium between phenol and phenolate forms. A very similar result was observed when **2** was added into a solution of of BSA in phosphate buffer (figure S7).

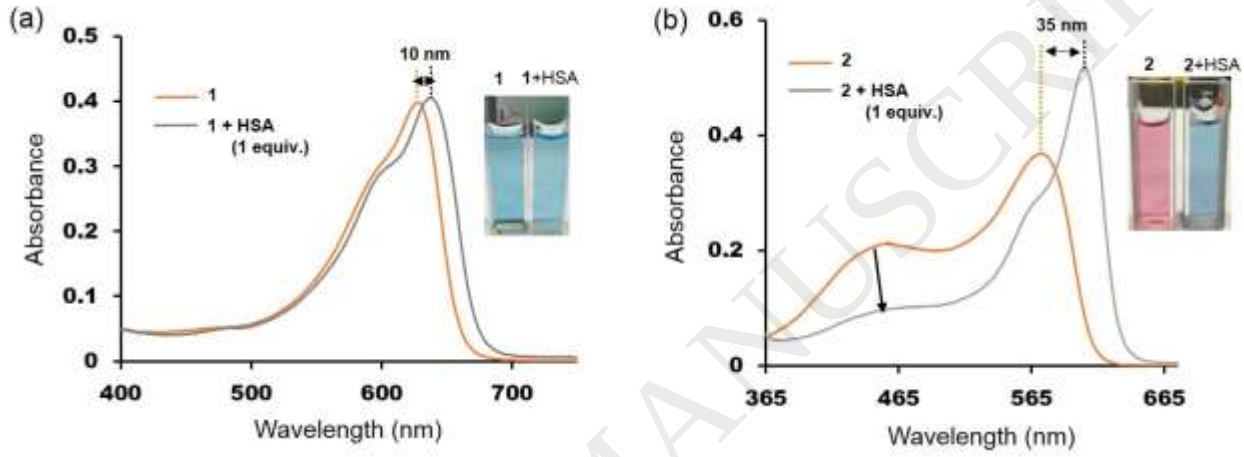

Figure 4. (a) Absorption spectra of **1** in buffer (pH = 7.4) and in presence of one equivalent of HSA. Inset: Color of **1** only in buffer and **1** with one equivalent of HSA in buffer. No visual color change was observed. (b) Absorption spectra of **2** in buffer (pH = 7.4) and in presence of one equivalent of HSA. Inset: Color of **2** only in buffer and **2** with one equivalent of HSA in buffer. Color change ($\Delta\lambda$ = 35 nm) was visible to the naked eyes.

Next, we studied the efficacy of the fluorophores for HSA detection in buffer and synthetic urine samples. The fluorophores were non fluorescent in phosphate buffer (1 mM, pH = 7.4) (figure 2c and 2d). However, upon addition of one equivalent of HSA emission dramatically increased, accompanied by red shift of the emission maxima (figure S8). A concentration dependent fluorimetric titration experiment revealed linear increase in emission intensity for both the fluorophores upon incremental addition HSA, which prompted us to calculate the association constant of the each fluorophore with HSA. As shown in figure 5, plot of $1/(I-I_0)$ *vs* 1/[HSA] (Benesi-Hildebrand equation) resulted a straight line, indicating 1:1 complex formation between the probes and HSA.[37] Moreover, the R^2 values for all the titrations suggest that a strong linear correlation exists between $1/(I-I_0)$ *vs* 1/[HSA] in the tested concentration range, also implying a

1:1 complex formation between the fluorophores and HSA (Scheme S2).[38-39] From the ratio of the slope and the intercept binding affinity was calculated and it was found to be $1.5 \pm 0.2 \times 10^5\ M^{-1}$ and $1.9 \pm 0.3 \times 10^5\ M^{-1}$ for **1** and **2**, respectively.

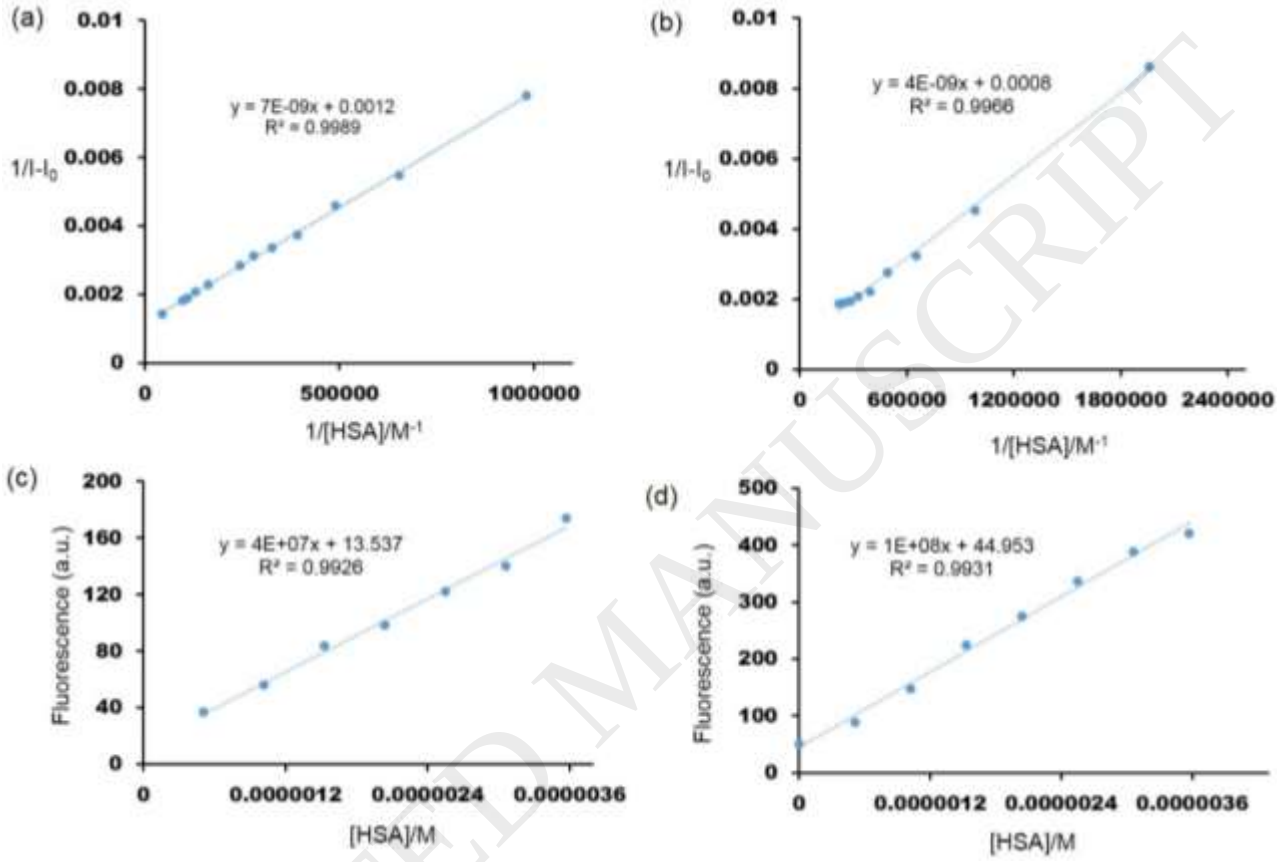

Figure 5. (a) Benesi-Hildebrand plot of $1/[I-I_0]$ vs $1/[HSA]$ (M^{-1}) for binding of **1** with HSA. (b) Benesi-Hildebrand plot of $1/[I-I_0]$ vs $1/[HSA]$ (M^{-1}) for binding of **2** with HSA. (c) Linear relationship between emission maxima of **1** and concentration of HSA. (d) Linear relationship between emission maxima of **2** and concentration of HSA.

Also, from the concentration dependent fluorescence data, limit of detection (LOD) was calculated in synthetic urine samples using IUPAC recommended 3σ/k equation and it was found to be 1.0±0.1 mg/L and 3.0±0.1 mg/L for **1** and **2**, respectively (figure 5c and 5d; Scheme S2).[40] Moreover, the emission intensity showed excellent correlation to the amount of HSA in synthetic urine samples, spanning in the range of ~33 mg/L to ~230 mg/L (figure 5c and 5d). The R^2 values more than 0.99 suggest that the amount of emission generated upon addition of each aliquot of HSA has an excellent linear correlation with the quantity of the HSA-fluorophore complex.

Therefore, these findings denote that both **1** and **2** can be used to quantitatively determine HSA in samples, both in normal and micro-albuminuria conditions. In this context it is important to highlight that **1** (LOD = 1.0 mg/L or 17 nM) lies in the detection limit ranges reported by Kumar *et. al*. (LOD = 11 nM) and Das *et. al*. (LOD ≈ 6.5 nM), and it shows lower LOD than other fluorophore based HSA sensors (Cheng. *et. al*., LOD= 140 nM; Xu. *et. al*., LOD = 140 nM; Ramezani *et. al*., LOD = 62 nM).[20-21, 41-43]

Fluorophore **1** showed excellent selectivity toward HSA. Fluorescence spectra of **1** and **2** were recorded in presence of different bio-macromolecules such as BSA (a protein structurally similar to HSA), β-lactoglobulin, γ-globulin (antibody isotype), and other biomolecules such as chicken egg albumin, hemoglobin, pepsin, trypsin, lysozyme, and insulin. Fluorescence of **1** dramatically increased only in presence of HSA. Other biomolecules including BSA had negligible effect on the fluorescence of **1** in physiological buffer (figure 6). On the contrary, probe **2** formed complex with BSA to same extent as to HSA. Also, one equivalent of β-lactoglobulin, γ-globulin, and chicken egg albumin enhanced the fluorescence of **2** to a great extent (figure 6).

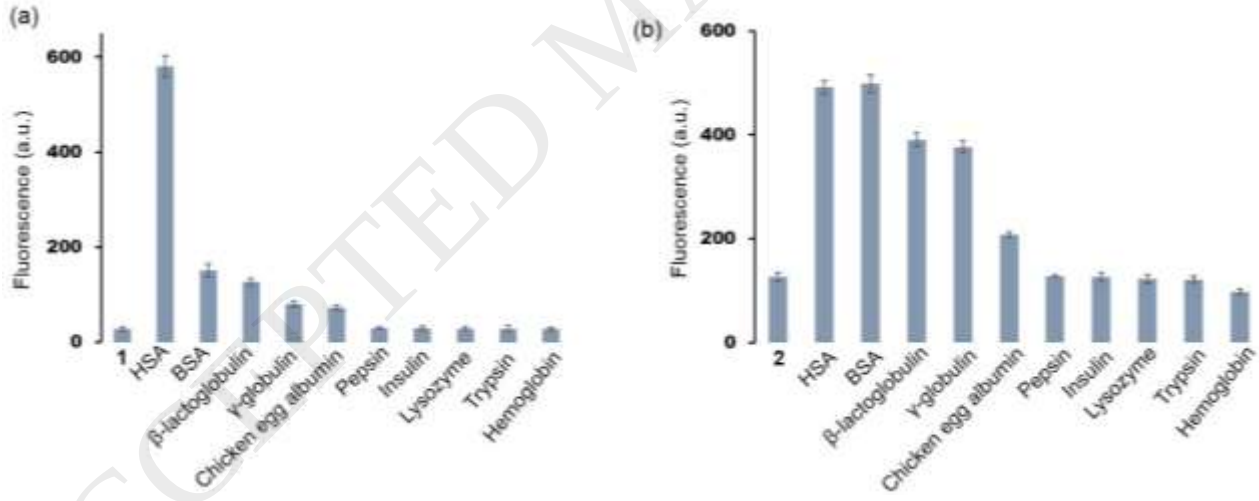

Figure 6. (a) Fluorescence response of **1** (10 μM) in presence of HSA and other biomacromolecules in phosphate buffer. (b) Fluorescence response of **2** (10 μM) in presence of HSA and other biomacromolecules in phosphate buffer.

These results demonstrate that fluorophore **1** selectively detects HSA; an important factor to consider during the development of a HSA specific small molecule based fluorimetric sensor. In this context, it should also be mentioned that binding of **1** with HSA was very rapid. Emission

increased rapidly and reached a saturation within less than a minute. Whereas, emission of **2** reached a saturation after ~5 minutes.

HSA consists three domains (domain I, II and III). Based on the several previous studies it has been established that it has two major drug binding sites, Sudlow I and Sudlow II. Sudlow I is located in domain II, whereas Sudlow II is located in domain III. In our study, mixing of HSA with the fluorophores enhanced their emissions in phosphate buffer, implying diffusion of the molecules and spontaneous formation of supramolecular complexes. To locate the binding site in the protein, two displacement assays were performed with known drugs, phenylbutazone and ibuprofen. Phenylbutazone binds in domain II ($K_a = 7.0 \times 10^5\ M^{-1}$) and ibuprofen binds in domain III ($K_a = 2.7 \times 10^6\ M^{-1}$).[44-45] As shown in figure 7, ibuprofen did not change the fluorescence signal of **1@**HSA. Addition of even excess (4 equiv.) drug did not interfere with the intensity of the signal, thus showing no influence on the interaction between **1** and HSA. Similar observations were noted for probe **2** (figure 7). However, addition of one equivalent of phenylbutazone, the site II marker, caused ~25% increase in the fluorescence intensity. With increasing amount of the drug, the intensity gradually increased. Upon addition of 5 equivalent of the drug, ~55% fluorescence enhancement was observed (figure S9). As probe **1** is non-fluorescent in buffer, the increase in intensity indicates that: (1) the drug displaces **1** from the original binding site, (2) **1** translates and binds in other areas of the protein when a competitive binder such as phenylbutazone is present in the solution. Similar phenomena were observed in the case of **2** (figure S9). In a separate study in phosphate buffer solution in the absence of HSA, phenylbutazone did not interfere with the emissions of the probes. Therefore, these displacement assays denote that the probes most likely bind at site II (Sudlow I).

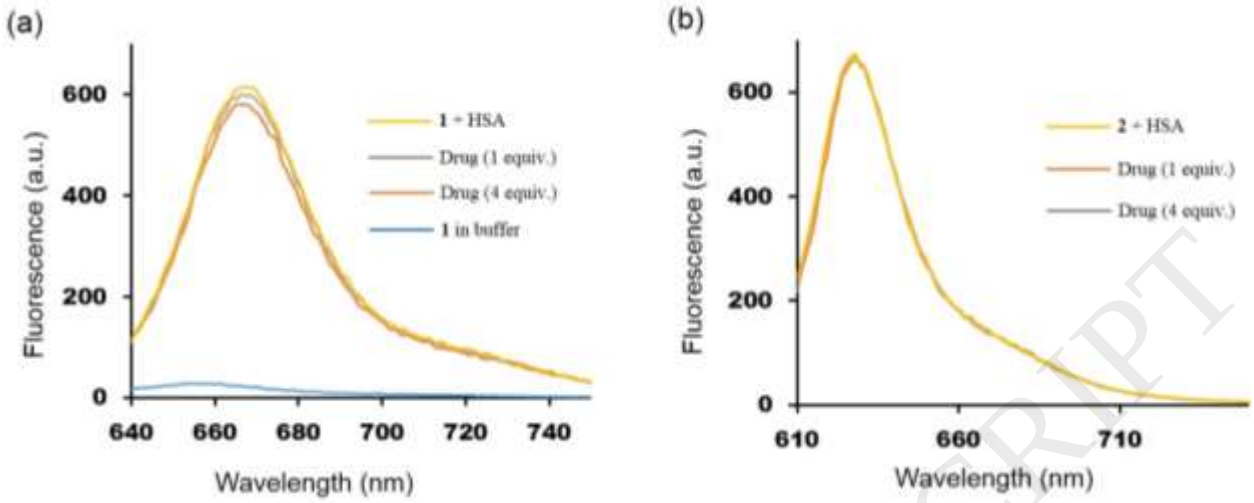

Figure 7. (a) Fluorescence spectra of **1**@HSA complex upon addition of different concentration of ibuprofen. (b) Fluorescence spectra of **2**@HSA complex upon addition of different amount of ibuprofen.

To further confirm the probe binding site in HSA, the emission of the aromatic amino acid tryptophan was monitored in the presence of **1**. Trp214 is located in site II (Sudlow I); it emits at 350 nm upon excitation with 285 nm of light. Usually, the microenvironment of the site affects the emission of the Trp214 residue. The intensity of emission decreases if a ligand is present in the site.[46] In our study, upon gradual addition of **1** in HSA, the emission intensity of the residue decreased. Addition of 0.4 equivalent of **1** quenched the emission up to ~30%. In the case of **2**, quenching was also observed, but to a greater extent. Addition of 0.4 equivalent of **2** reduced the emission intensity to half of the original value (figure S10). Moreover, these fluorophores had no effect on the emission of commercial tryptophan when studied separately in only phosphate buffer solutions (figure S11). Thus, these findings suggest that the probes bind preferentially in Sudlow I (site II), most likely driven by hydrophobic and van der Waals interactions.[47-48]

Molecular docking studies were performed to gain a visual perspective of the fluorophore-HSA binding and to understand the types of fluorophore-residue interactions in the binding site. The 3D structure of HSA was obtained from protein data bank (PDB code: 2BXC). Dockings were carried out with AutoDock Vina program.[32] Total eight structures were generated and ranked from lowest to highest binding affinities.

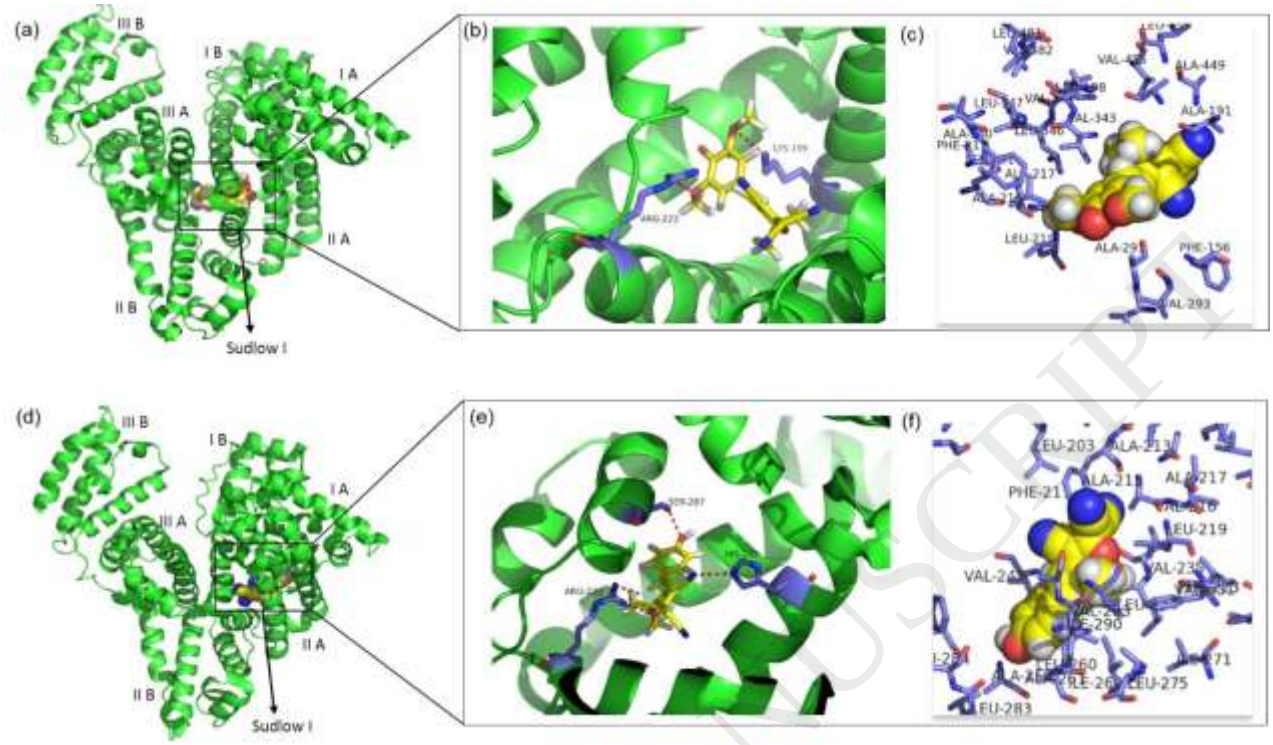

Figure 8. (a) Docking conformation of **1**@HSA complex of the lowest binding affinity. (b) Hydrogen bonding interactions between **1** and HSA are shown as dotted red lines. (c) Hydrophobic residues and favorable interactions accommodate **1** within HSA. (d) Docking conformation of **2**@HSA complex of the lowest binding affinity. (e) Hydrogen bonding interactions between **2** and HSA are shown as dotted red lines. (f) Hydrophobic residues and favorable interactions accommodate **2** within HSA.

Figure 8 depicts the best binding pose between the fluorophore and the HSA. Fluorophore **1** binds at the entrance of the pocket (at Sudlow I), interacting with two residues (Lys199 and Arg222) (figure 8a and 8b). In Lys199 the side chain classified as basic remains charged at physiological pH. Arg222 has both hydrophobic and hydrophilic groups and a positively charged guanidinium group at the end of the hydrophobic side chain. As shown in figure 8b, both Lys199 and Arg222 form hydrogen bonds with the methoxy groups of **1**. Lys199 and Arg222 are located on the outer surface of the pocket entrance. Therefore, the lowest energy docked conformation as well as the specific hydrogen bonding interactions with these residues indicate that **1** is not deeply buried within the cavity, and its TCF part is located between the area of domain II and III (figure 8a and 8b). Moreover, several hydrophobic residues such as ALA, LEU, and PHE interact with the probe

by hydrophobic interactions (figure 8c). Whereas, in the case of **2**, residue Ser287, a polar amino acid with a hydroxyl group at the end of the aliphatic chain, forms hydrogen bond with the phenolic –OH group, and Histidine (His242) with positively charged imidazole group interacts with nitrogen atom of the nitrile group (figure 8d and 8e). Unlike **1**, Arg222 shows two hydrogen bonding interactions with the acceptor moiety of **2**, one with the nitrogen atom of the nitrile group and another with the oxygen atom of the furan group (figure 8e). His 242 is located at the bottom of the pocket (Sudlow I). Therefore, hydrogen bonds between the acceptor moietie of the **2** with the His242 indicates that it is deeply buried within the cavity (figure 8d). Moreover, probe 2 also interacts with several hydrophobic residues such as ALA, LEU, PHE, and VAL in the binding site (figure 8f). Overall, the molecular docking studies suggest that the probes were bound at the Sudlow I by hydrogen bonds and hydrophobic interactions (figure 8). Moreover, the docked structures were supported by the molecular displacement studies with the site specific drug molecules as well as by the intrinsic tryptophan fluorescence quenching studies.

From the experimental and theoretical studies the selective response of **1** toward HSA can be attributed to its steric features and specific interactions with the surrounding amino acids. Due to the presence of two methoxy groups at ortho positions **1** could not completely enter the binding site (site IIA), and it resides between site IIA and IIIA. We believe that the fluorescence enhancement of **1** upon binding within the pocket is due to the increased hydrophobic and van der Walls interactions, reducing the rotational motions of **1** in the pocket. To confirm that the micro-environment could result enhanced charge transfer fluorescence for **1**, emission studies were carried out in several glycerol/water mixtures. As shown in figure S13, upon gradual increase of the amount of glycerol in a glycerol-water mixture, the emission intensity of **1** increased along with a bathochromic shift of the maxima. A ten times emission enhancement was observed just with 9:1 glycerol/water (η = 267 cP at 25 ^{o}C) mixture. This phenomenon could be attributed to the restricted rotational motion of **1** within a highly viscous environment, thereby reducing the excited state energy loss via non-radiative pathways. Moreover, though addition of glycerol in water reduces the polarity of the medium, a 12 nm bathochromic shift of the emission was observed in the 9:1 glycerol/water mixture.

Whereas with BSA, **1** formed loosely bound complex within an unconventional site (between domain I and III, figure S14a). From the absorption studies (figure S14b) a ground state complex

formation can be proposed. However, poor interactions with the amino acids at this site most likely have caused a weak fluorescence enhancement. Only five times increase in emission intensity was observed with BSA, whereas it was 20 times with HSA. From the molecular docked models and the strong correlation between micro-viscosity with the emission of **1**, we estimate that multiple interactions at a smaller volume within HSA severely reduced intramolecular rotational motions of **1**, resulting a selective response to HSA. In case of BSA, this effect was marginal as **1** formed complex at a more open and larger site of the HSA.

In this context, it should also be mentioned that **2** was deeply buried within the site IIA of HSA, interacting with basic amino acids (figure 8d). Therefore, it is likely that a basic residue deprotonates the phenolic –OH, and hence a large red shift (~ 35 nm) of absorption maxima was observed when HSA was added into the solution of **2** at physiological buffer (figure 4).[49]

Conclusions

Two donor-acceptor fluorophores were prepared and studied for selective detection of HSA in aqueous samples. Both fluorophores were emissive in non-polar solvents. But, the emission was quenched in polar solvents due to energy loss via non-radiative pathways. The emission was further quenched in a buffer solution (pH = 7.4) due to deprotonation of the phenolic –OH, which most likely led to a better population as well as stabilization of the charge transfer states. However, the emission could be recovered within a viscous microenvironment. Upon addition of glycerol in an aqueous solution of **1**, multifold emission enhancement along with bathochromic shift of the maxima was observed. Similar emission enhancement was observed within the proteins' microenvironment. Both fluorophores displayed high complexation affinity and strong "turn-on" fluorescence response with HSA, which resulted an impressive limit of detection for both the fluorophores (LOD; 1.0±0.1 mg/L and 3.0±0.1 mg/L for **1** and **2**, respectively) in HSA spiked synthetic urine solutions.

Fluorophore **1** selectively responds to HSA. The selectivity of **1** was established by comparing the emission of **1**@HSA with other proteins and biomolecules such as BSA, β-lactoglobulin, γ-globulin, chicken egg albumin, etc. Fluorophore **2** however could not distinguish between HSA and BSA. Its emission signal in BSA was as intense as **1**@HSA in identical experimental conditions. Moreover, it displayed strong "turn-on" fluorescence response in presence of other

proteins such as β-lactoglobulin, γ-globulin, and chicken egg albumin. The high selectivity of **1** toward HSA can be attributed to its different size and shape and the strong interactions with the amino acids within the narrow microenvironment.

Different classes of donor-acceptor fluorophores have been studied extensively in different branches of science and technology. Many such fluorophores are commercially available and currently in use in medical and health science research. We believe that the donor-acceptor fluorophores of pH sensitive phenol derivatives will provide a new promising platform for tuning absorption and emission profiles of new NIR fluorophores for selective biosensing and cellular imaging.

Declarations of interest

None

Acknowledgements

This work was supported by the IDeA Networks of Biomedical Research Excellence (INBRE) grant (grant number P20GM 103429).

Supplementary data

Details of the synthesis of the probes, ^{1}H and ^{13}C NMR, photostability study under visible light, and additional spectra. This material is available online via www.elsevier.com.

References

1. G. J. Quinlan, G. S. Martin, T. W. Evans, *Hepatology*, 2005, **41**, 1211-1219.
2. T. Peters. *All about albumin: biochemistry, genetics, and medical applications.* Academic Press Inc., San Diego, USA, 1996.
3. B. T. Doumas, T. Jr. Peters, *Clin. Chim. Acta,* 1997, **258**, 3-20.
4. S. Arques, P. Ambrosi, *J. Card. Failure,* 2011, **17**, 451-458.
5. G. Fanali, A. di Masi, V. Trezza, M. Marino, M. Fasano, P. Ascenzi, *Mol. Aspects Med*. 2012, **33**, 209-290.
6. V. J. Alino, K. L. Yang, *Analyst*, 2011, **136**, 3307-3313.
7. K. Hoogenberg, W. J. Sluiter, R. P. Dullaart, *Acta Endocrinol*., 1993, **129**, 151-157.
8. D. Zeeuw, H. H. Parving, R. Henning, *J. Am. Soc. Nephrol.,* 2006, **17**, 2100-2105.

9. R. Amin, B. Widmer, A. T. Prevost, P. Schwarze, J. Coope, J. Edge, L. Marcovecchio, A. Neil, R. N. Dalton, D. B. Dunger, *Br. Med. J*., 2008, **336**, 697-701.

10. H. Thakkar, D. J. Newman, F. Holownia, C. L. Davey, C. C. Wang, J. Lloyd, A. R. Craig, C. P. Price, *Clin. Chem*. 1997, **43**, 109−113.

11. Z. Z. Huang, H. N. Wang, W. S. Yang, *Appl. Mater. Interface*, 2015, **7**, 8990–8999.

12. H. X. Sun, J. F. Xiang, X. F. Zhang, H. B. Chen, Q. F. Yang, Q. Li, A. J. Guan, Q. Shang, Y. L. Tang, G. Z. Xu, *Analyst*, 2014, **139**, 581–584.

13. R. E. Wang, L. Tian. Y. Chang, *J. Pharm. Biomed. Anal.*, 2012, **63**, 165-169.

14. D. Caballero, E. Martinez, J. Bausells, A. Errachid, J. Samitier, *Anal. Chim. Acta.*, 2012, **720**, 43–48.

15. M. C. Tu, Y. Z. Chang, Y. T. Kang, H. Y. Chang, P. Chang, T. R. Yew, *Biosens. Bioelectron.*, 2012, **34**, 286–290.

16. Y. Ermolenko, A. Anshakova, N. Osipova, M. Kamentsev, O. Maksimenko, V. Balabanyan, S. Gelperina, *J. Pharmacol. Toxicol. Methods*, 2017, **85**, 55–60.

17. R. Singh, F. W. Crow, N. Babic, W. H. Lutz, J. C. Lieske, T. S. Larson, R. A. Kumar, *Clin. Chem*., 2007, **53**, 540–542.

18. X. D. Zeng, M. S. Ma, B. C. Zhu, L. A. Zhu, *Anal. Sci*., 2016, **32**, 1291–1294.

19. K. Rajasekhar, J. A. Chaithra, T. Govindaraju, *Org. Biomol. Chem*., 2017, **15**, 1584-1588.

20. S. Samanta, S. Halder, G. Das, *Anal. Chem*., 2018, **90**, 7561-7568.

21. S. I. Reja, I. A. Khan, V. Bhalla, M. Kumar, *Chem. Commun*., 2016, **52**, 1182−1185.

22. R. Choudhury, H. E. Parker, C. M. Cendejas, K. L. Mendenhall, *Tet. Lett*., **2018**, 59, 3020-3025.

23. G. Hong, A. L. Antaris, H. Dai, *Nat. Biomed. Eng*., 2017, **1**, 1-22.

24. K. A. Willets, O. Ostroverkhova, M. He, R. J. Twieg, W. E. Moerner, *J. Am. Chem. Soc.* 2003, **125**, 1174-1175.

25. W. E. Moerner, R. J. Tweig, D. W. Kline, M. He, U.S. Patent 20070134737A1. 2007.

26. H. Wang, Z. Lu, S. J. Lord, W. E. Moerner, R. J. Twieg, *Tet. Lett*., 2007, **48**, 3471-3474.

27. J. Fabian. *Chem. Rev*., 1992, **92**, 1197-1228.

28. C. Staudinger, S. M. Borisov, *Methods Appl. Fluoresc*., 2015, 042005.

29. F. Bureˇs. *RSC Adv*., 2014, **4**, 58826-58851.

30. J. R. Lakowicz. *Principles of Fluorescence Spectroscopy*, Springer, New York, 2011.

31. Z. R. Grabowski, K. Rotkiewicz, *Chem. Rev*., 2003, **103**, 3899-4031.

32. O. Trott, A. J. Olson, *J. Comput. Chem*., 2009, **31**, 455-461.

33. M. W. Wu, K. Li, C. Y. Li, J. T. Hou, X. Q. Yu, *Chem. Commun*., 2014, **50**, 183-185.

34. M. Ipuy, C. Billon, G. Micouin, J. Samarut, C. Andraud, Y. Bretonniere, *Org. Biomol. Chem*., 2014, **12**, 3641-3648.

35. F. A. S. Chipen, A. Mishra, G. Krishnamoorthy, *Phys. Chem. Chem. Phys*., 2012, **14**, 8775-8790.

36. B. Wandelt, P. Turkewitsh, B. R. Stranix, G. D. Darling, *Faraday Trans*., 1995, **91**, 4199-4205.

37. H. A. Benesi, J. H. Hildebrand, *J. Am. Chem. Soc*., 1949, **71**, 2703-2707.

38. R. B. Singh, S. Mahanta, A. Bagchi, N. Guchait, *Photochem. Photobiol. Sci*., 2009, **8**, 101-110.

39. S. Nigam, D. Gurocher, *J. Phys. Chem*. 1996, **100**, 7135-7142.

40. G. L. Long, J. D. Winefordner, *Anal. Chem*., 1983, **55**, 712-724.

41. T. Gao, S. Yang, X. Cao, J. Dong, N. Zhao, P. Ge, W. Zeng, Z. Cheng, *Anal. Chem*., 2017, **89**, 10085−10093.

42. X. Fan, Q. He, S. Sun, H. Li, Y. Pei, Y. Xu, *Chem. Commun.*, 2016, **52**, 1178−1181.

43. A. M. Ramezani, J. L. Manzoori, M. Amjadi, A. Jouyban, *Sci. World J*., 2012, **2012**, 1-9.

44. N. E. Basken, G. J. Mathias, M. A. Green, *J. Pharm. Sci*., 2009, **98**, 2170-2179.

45. I. Petitpas, A. A. Bhattacharya, S. Twine, M. East, S. Curry, *J. Biol. Chem*., 2001, **276**, 22804-22809.

46. Y. Yu, Y. Huang, F. Hu, Y. Jin, G. Zhang, D. Zhang, R. Zhao, *Anal. Chem.*, 2016, **88**, 6374-6381.

47. V. Lhiaubet-Vallet, Z. Sarabia, F. Bosca, M. A. Miranda. *J. Am. Chem. Soc*., 2004, **126**, 9538-9539.

48. M. C. Jimenez, M. A. Miranda, I. Vaya, *J. Am. Chem. Soc*., 2005, **127**, 10134-10135.

49. S. Ito, D. Yamamoto, Biomed. Res., 2015, **36**, 247-252.